Available online at www.sciencedirect.com
ScienceDirect
Journal of Power Sources 173 (2007) 887–890
JOURNAL OF POWER SOURCES
www.elsevier.com/locate/jpowsour

Short communication

Measurement of partial oxygen ion conductivity of Sr-doped lanthanum manganite

Wenhua Huang, Srikanth Gopalan *, Uday Pal

Department of Manufacturing Engineering, Boston University, 730 Commonwealth Ave., Boston, MA 02215, United States

Received 16 January 2007; received in revised form 30 May 2007; accepted 4 June 2007
Available online 23 June 2007

Abstract

Sr-doped lanthanum manganite (LSM) is considered to be a suitable cathode material for solid oxide fuel cells (SOFC). Presently, bi-layer dense structures of p-type LSM on n-type perovskite oxides are being considered for application as SOFC interconnections. In this paper, we have measured the partial oxygen ion conductivity of LSM, an important property that is crucial to the design of such interconnections. Dense LSM was successfully deposited on sintered yttria-stabilized zirconia (YSZ) plates by DC-magnetron sputtering. The oxygen-ion conductivity of LSM was measured as a function of oxygen partial pressure, pO_2, by using the YSZ as an electron blocking method in the temperature range between 680 and 880 °C.

Keywords: Fuel cell; Lanthanum manganite; Partial conductivity

1. Introduction

Sr-doped lanthanum manganite (LSM) is considered to be a suitable cathode material for solid oxide fuel cell (SOFC) because of its high electronic conductivity, high catalytic activity for oxygen reduction, and chemical and mechanical compatibility with solid electrolytes based on yttria-stabilized zirconia [1–5]. Conceptually it can also be employed as the p-type layer of an n–p-type bi-layer interconnection in SOFCs as shown in Fig. 1. In an actual device, the p-type layer of the bi-layer interconnection will be exposed to an oxidizing environment and the n-type layer to reducing conditions. During operation of the cell, the layer exposed to oxidizing conditions (cathodic side) will develop p-type conductivity and the layer exposed to reducing conditions (anodic side) will develop n-type conductivity. If designed appropriately, such a structure has the potential to remain chemically stable and serve as an excellent SOFC interconnection, maintaining a high electronic conductivity across its thickness [6]. Apart from the high electronic conductivity, the requirements for the bi-layer interconnection are low oxygen ion conductivity and excellent stability in the high oxygen partial pressure gradient present across the anodic and cathodic chambers. To engineer the thicknesses of each layer in the bi-layer interconnection structure for chemical stability in the dual (anodic and cathodic) atmosphere, it is important to measure the partial oxygen-ion conductivities in the individual layers as a function of oxygen partial pressure, pO_2.

Yasuda measured the oxygen tracer diffusion coefficient of sintered LSM, which includes the compositions most frequently used as cathodes for SOFCs, as a function of composition, temperature and oxygen partial pressure [7]. Belzner measured the chemical diffusion coefficient of oxygen in strontium-doped lanthanum manganites using potentiostatic step method [8]. The oxide ionic conductivity was also calculated based on chemical diffusion of oxygen and permeation measurements [9–11]. However, experimental data is not readily available on oxygen ionic conductivity of LSM thin film as a function of temperature and oxygen partial pressure.

In this paper, we have evaluated the oxygen-ion conductivity of LSM thin film as a function of oxygen partial pressure by using an electron-blocking method in the temperature range between 680 and 880 °C. Dense Sr-doped lanthanum manganite films were deposited on polycrystalline oxygen-ion conducting yttria-stabilized zirconia (YSZ) plates by DC-magnetron sput-

* Corresponding author. Tel.: +1 617 358 2297; fax: +1 617 353 5548.
E-mail address: sgopalan@bu.edu (S. Gopalan).

0378-7753/$ – see front matter © 2007 Published by Elsevier B.V.
doi:10.1016/j.jpowsour.2007.06.068

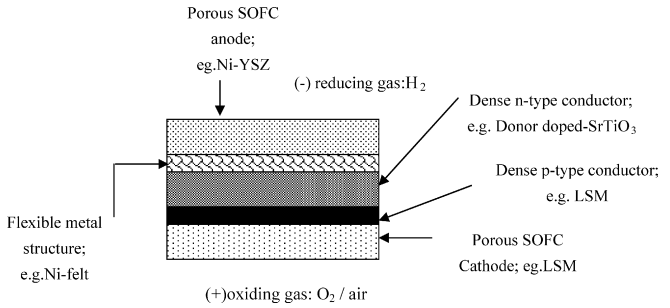

Fig. 1. Bi-layer interconnection repeat element; the electrolyte of the SOFC is not shown in the figure.

tering and the conductivity was measured with a small DC bias (5–20 mV) across the bi-layer sample.

2. Experimental details

2.1. Target preparation

Powder of nominal composition $La_{0.85}Sr_{0.15}MnO_3$ (LSM) was prepared by the solid state reaction method. Stoichiometric mixtures of La_2O_3 (99.99%), $SrCO_3$ (99%), Mn_2O_3 (99.9%) were calcined at 1200 °C. The calcined powders were crushed and ball-milled, after which this procedure was repeated. The fine LSM powders were uniaxially pressed in a cylindrical die to obtain a sample of diameter 60 mm and thickness of 5 mm to be used as a target in DC magnetron sputtering experiments. The sample was sintered in air at 1450 °C for 10 h.

2.2. Deposition of LSM film by DC magnetron sputtering

Yttria-stabilized zirconia (8YSZ) powder, purchased from Tosoh USA, was pressed into pellets and sintered at 1500 °C for 4 h. The pellets were polished using 0.25 μm diamond paste. Prior to film deposition, the substrates were successively rinsed in de-ionized water, ultrasonically cleaned in acetone and finally dried with dry nitrogen, before loading into the deposition chamber. The deposition chamber was then evacuated to a base pressure below 5×10^{-6} Torr when the liquid-nitrogen trap was filled. Sputtering was conducted in a 99.999% pure argon atmosphere. The argon pressure was 4 mTorr. The substrates were not intentionally heated during deposition, but the substrate temperature rose to around 70 °C during deposition under typical conditions. A constant current of 0.5 A was applied to the target

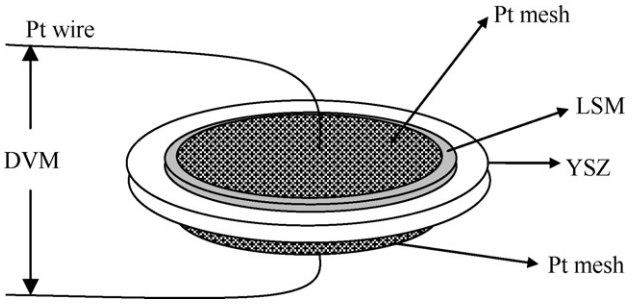

Fig. 2. Schematic of the specimens.

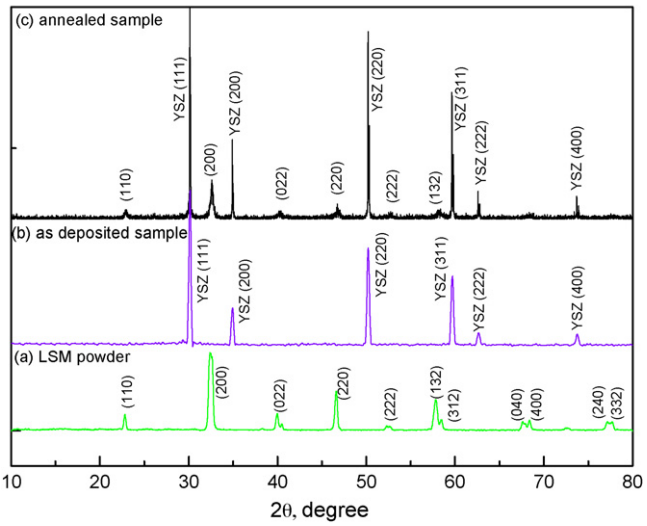

Fig. 3. XRD patterns of the (a) LSM powder, (b) as deposited film and (c) films which is annealed at 1000 °C for 10 h.

at a DC voltage of 195–200 V prior to film deposition. The targets were sputter-cleaned for 10 min with a shutter covering the substrates.

The deposition was conducted for 2–5 h which produced 2–5 μm thick films. Deposition rates of up to 1 μm h^{-1} could be easily obtained with this magnetron sputtering equipment. After deposition, the samples were annealed in air at 1000 °C for 10 h then cooled slowly to room temperature.

2.3. Characterization

The target and the thin films were characterized by X-ray diffraction (XRD) using a Rigaku diffractometer with Cu Kα radiation. Scanning electron microscopy (SEM) and wavelength-dispersive spectrometry (WDS) were used to determine the morphology and the composition of the deposited films.

2.4. Oxygen-ion conductivity measurement

A method analogous to the Hebb–Wagner (H–W) method is used to determine the oxygen ionic conductivity of La(Sr)MnO_3(LSM). The cell used is schematically give as:

$$Pt(O_2)/YSZ\,(1\,mm)/La(Sr)MnO_3\,(4\,\mu m)/Pt(O_2)$$

where the yttria-stabilized zirconia is used as a blocking layer to block the electronic current through the LSM during steady-state DC measurements under a small applied potential. Then, $R_i = V/I$, where V is the applied voltage, I is the measured current through the cell and R_i is the total ionic resistance of the cell [12]. Similar to the H–W method, in this configuration, the resistance of the 1 mm thick YSZ pellet to electronic current is much larger than the resistance of the 4 μm thick LSM layer to ionic current, i.e., $(R_{el}^{YSZ} = \rho_{el}^{YSZ} L^{YSZ}) \gg (R_i^{LSM} = \rho_i^{LSM} L^{LSM})$. For instance, at 800 °C and in an oxygen partial pressure of $pO_2 = 10^{-4}$ atm, the electronic resistance, R_{el}^{YSZ} of

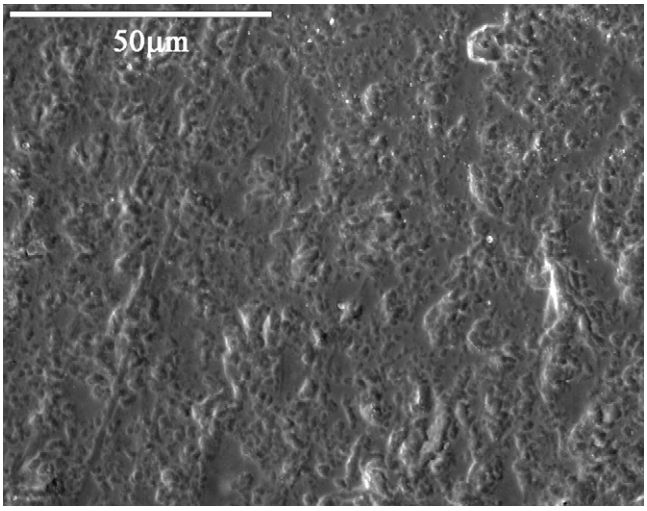

Fig. 4. The SEM photographs of the sputtered LSM film on a YSZ substrate.

a 1 mm thick YSZ pellet is $3.2 \times 10^5\ \Omega\,cm^2$ and the ionic resistance of a 4 μm thick LSM layer, R_i^{LSM} is $6.76 \times 10^3\ \Omega\,cm^2$ [9,13]. In the preceding discussion, R_{el}^{YSZ} represents the area-specific electronic resistance of YSZ in $\Omega\,cm^2$, ρ_{el}^{YSZ} represents the electronic resistivity of YSZ in Ω cm, L^{YSZ} represents the thickness of the YSZ pellet in cm, R_i^{LSM} represents the area-specific ionic resistance of LSM in $\Omega\,cm^2$, ρ_i^{LSM} represents the ionic resistivity of LSM in Ω cm and L^{LSM} represents the thickness of LSM layer in cm.

In blocking electrode experiments there is always the question of which layer is functioning as the blocking layer, i.e. whether the electronic current is being blocked by the YSZ layer or the ionic current by the LSM layer. As shown above, based on preliminary data available in the literature and the thicknesses of the two layers, it is clearly that the electronic resistance of the YSZ layer far exceeds the ionic resistance of the LSM layer. Thus, the YSZ pellet functions as the electron blocking layer.

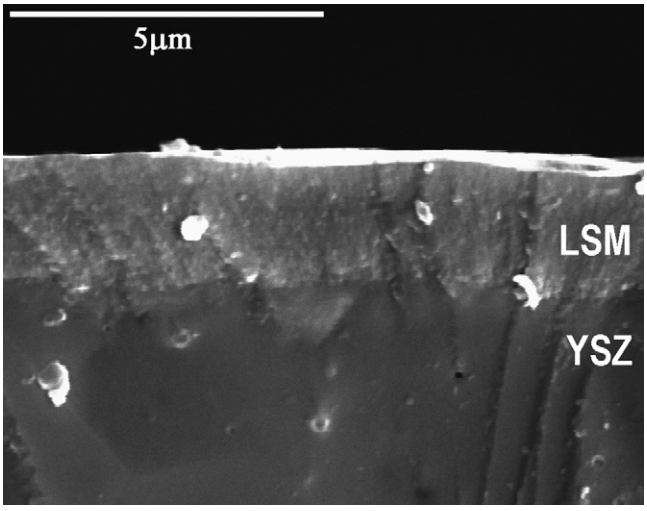

Fig. 5. The SEM photographs of the cross sections of sputtered LSM film on a YSZ.

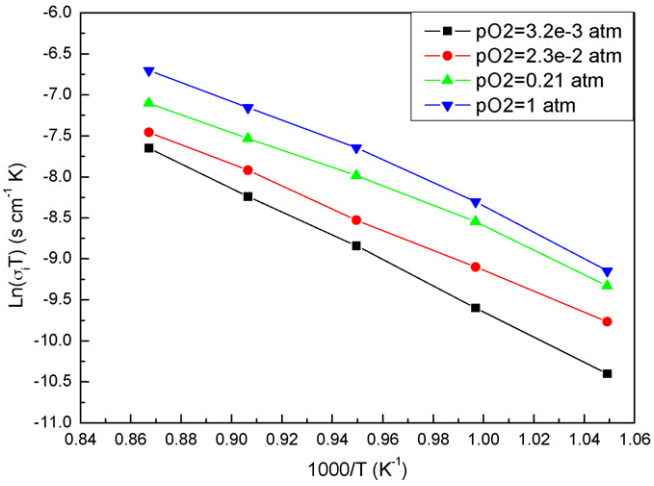

Fig. 6. Temperature dependence of the oxygen ion conductivity of LSM.

The configuration of the test specimen is shown in Fig. 2. LSM films were deposited by DC magnetron sputtering as described above. Mixtures of O_2, N_2 and Ar/H_2 were to control oxygen partial pressure. Oxygen partial pressure was monitored in situ by a zirconia oxygen sensor in the experimental chamber.

2.5. XRD, SEM, and WDS results

Fig. 3 shows representative XRD spectra from the LSM powder, 2 μm-thick films as-deposited by DC magnetron sputtering and the same film, which is annealed at 1000 °C for 10 h. The XRD indicates that the powder (a) has a single-phase of pseudo-tetragonal structure. The as-deposited film (b) was amorphous as indicated by the lack of any reflections from the perovskite phase and only appearance of the peaks of the YSZ substrate. The crystallinity of this sample improved after annealing at 1000 °C for 10 h (c) as indicated by the appearance of LSM peaks. The XRD pattern of the LSM film is the same as that of the powdered sample except for the intensity ratio.

The morphology and microstructure of the films in the micrometer range was investigated by SEM. Figs. 4 and 5 show the surface view and the fractured cross-section of the sputtered LSM on YSZ substrate, which was annealed at 1000 °C for 10 h after deposition. It indicates that the LSM film is crack-free, very dense and well-bonded to the YSZ substrate, which is important from the standpoint of measuring the ionic conductivity of the LSM film.

Table 1 shows the chemical composition of film deposited by DC magnetron sputtering and targets analyzed by WDS. The chemical composition of the resultant film is slightly different from the target composition.

Table 1
Chemical composition of film deposited by DC magnetron sputtering and target analyzed by WDS

	Film	Target
Sample	$La_{0.96}Sr_{0.08}MnO_{2.991}$	$La_{0.87}Sr_{0.157}MnO_{2.987}$

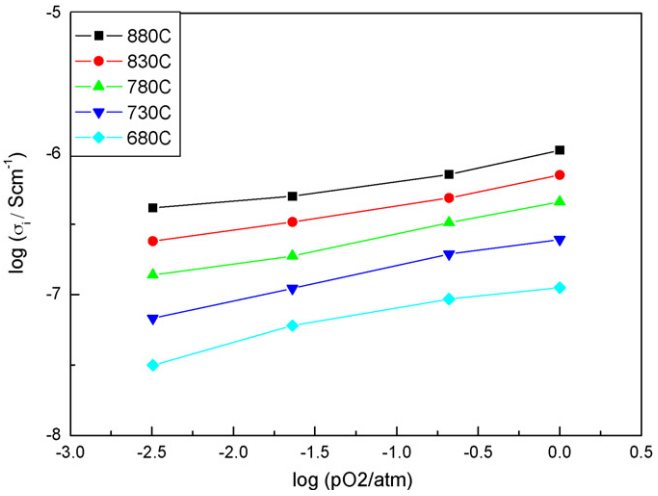

Fig. 7. The oxygen partial pressure dependence of the oxygen ion conductivity of LSM.

The oxygen ion conductivity of LSM was measured using a method analogous to the H–W method as described in Section 2.4. Independent conductivity and transport number measurements show that the ionic resistance of the YSZ plate is only around 0.2–3% of the total measured resistance in our experiments, i.e. the largest part of the total resistance is the oxygen ion resistance of LSM. So, in this paper, the total resistance of the cell was used to calculate the oxygen ion conductivity of LSM. The temperature dependence of the oxygen ion conductivity of LSM at different oxygen partial pressure is shown in Fig. 6. The relationship between the $\ln \sigma_i T$ and $1/T$ showed an expected linear relationship. The value of the activation energy of the oxygen ion conductivity is slightly different at different oxygen partial pressures. The activation energy of the oxygen ion conductivity in air is about 101 kJ mol^{-1}.

The oxygen partial pressure dependence of the oxygen ion conductivity of LSM is shown in Fig. 7. As shown here, the oxygen ionic conductivity was almost proportional to the 1/5 power of the oxygen partial pressure at the higher range from 10^{-3} to 1 atm. This is different from the dependence expected from the oxygen vacancy diffusion mechanism in which oxygen vacancies are considered to control the ionic diffusion. The oxygen non-stoichiometry measured by Mizusaki et al. [14] has a weak pO_2 dependence in the pO_2 range of 10^{-3} to 1 atm. Therefore, the dependence observed in this measurement is most likely not related to the pO_2 dependence of oxygen vacancy concentration in LSM, but due to the diffusion of oxide ions through grain boundaries.

A similar phenomenon was observed in doped lanthanum chromite thin films. Lanthanum chromite is also a p-type semiconductor [15]. The value of oxygen ion conductivity measured at 880 °C in air is 7.1×10^{-7} S cm^{-1}, which is of the same order of magnitude as determined by isotope diffusion measurements [7].

3. Conclusions

Dense Sr-doped lanthanum manganite (LSM) films were deposited on polycrystalline oxygen-ion conducting yttria-stabilized zirconia (YSZ) plates by DC-magnetron sputtering. A method analogous to the H–W method is used to determine the oxygen ionic conductivity of La(Sr)MnO_3. In the oxygen partial pressure range of 10^{-3} to 1 atm, the ionic conductivity ranges from $10^{-7.3}$ to 10^{-6} S cm^{-1}.

Acknowledgements

The authors would like to thank Professor Vinod K. Sarin for providing access to the DC-magnetron sputtering machine. The authors also thank Dr. Guoshen Ye for assistance with the SEM.

References

[1] N.Q. Minh, J. Am. Ceram. Soc. 76 (1993) 563.
[2] T. Inoue, K. Eguchi, T. Setoguchi, H. Arai, Solid State Ionics 40–41 (1990) 407.
[3] A. Hammouche, E. Siebert, A. Hammou, Mater. Res. Bull. 24 (1989) 367.
[4] O. Yamamoto, Y. Takeada, R. Kanno, M. Noda, Solid State Ionics 22 (1987) 241.
[5] Y. Takeda, R. Kanno, M. Noda, Y. Tomida, O. Yamamoto, J. Electrochem. Soc. 134 (1987) 2656.
[6] W. Huang, S. Gopalan, Solid State Ionics 177 (2006) 347.
[7] I. Yasuda, K. Ogasawara, M. Hishinuma, T. Kawada, M. Dokiya, Solid State Ionics 86–88 (1996) 1197.
[8] A. Belzner, T.M. Gur, R.A. Huggins, Solid State Ionics 57 (1992) 327.
[9] A. Endo, M. Ihara, H. Komiyama, K. Yamada, Solid State Ionics 86–88 (1996) 1191.
[10] H. Ullmann, N. Trofimenko, F. Tietz, D. Stover, A. Ahmad-Khanlou, Solid State Ionics 138 (2000) 79.
[11] A. Endo, H. Fukunaga, C. Wen, K. Yamada, Solid State Ionics 135 (2000) 353.
[12] P.J. Gellings, H.J.M. Bouwmeester, Handbook of Solid State Electrochemistry, CRC Press, Boca Raton, FL, 1997, p. 248.
[13] J.H. Park, R.N. Blumenthal, J. Electrochem. Soc. 136 (1989) 2867.
[14] J. Mizusaki, H. Tagawa, K. Naraya, T. Sasamoto, Solid State Ionics 49 (1991) 111.
[15] M. Suzuki, H. Sasaki, A. Kajimura, Solid State Ionics 96 (1997) 83.